ON THE EVALUATION OF ICE MODELS

D. Sulsky[1], K. Peterson[1], H. Schreyer[1], R. Kwok[2] and M. Coon[3]
[1] University of New Mexico, Albuquerque NM 87131, USA
[2] Jet Propulsion Laboratory, Pasadena, CA 91109, USA
[3]Northwest Research Associates, Seattle, WA 98009, USA

ABSTRACT

A method is presented for an evaluation of coupled dynamic and thermodynamic ice models using the RADARSAT Geophysical Processor System (RGPS) data and products for validation. The technique has been applied to a standard viscous-plastic rheology with a simple two-level ice thickness model for three test regions of the Arctic pack ice. High correlation is obtained between observed and predicted ice speeds. The model predictions show reasonable correlation with the data when examining shear and vorticity, but poorer correlation with divergence. The amount of opening is under predicted in these simulations.

INTRODUCTION

In recent years, the availability of large volumes of recorded ice motion data, derived from high-resolution Synthetic Aperature Radar (SAR) imagery, has provided an amazingly detailed look at the deformation of the ice cover. Three-day SAR observations of the western Arctic Ocean have been acquired since November, 1996, and data acquisition continues. These observations are processed by the RADARSAT Geophysical Processor System (RGPS), a data analysis system developed at JPL that assembles the sequential SAR images into basinwide fields of ice motion and deformation, and additionally estimates ice age and thickness. RGPS procedures track material elements (cells) of sea ice in SAR imagery over time, allowing us to follow their location and deformation history [Kwok et al., 1995; Kwok, 1998]. Thus, from the RGPS products, we obtain repeated 3-day observations of the motion and deformation of each cell.

These remarkable data put us in a position to begin detailed evaluation of current coupled mechanical and thermodynamic models of sea ice. These models are composed of constitutive models that govern the mechanical behavior of ice, and thickness distribution models that govern the thermodynamic aspects. Numerical simulations of ice dynamics typically make use of a viscous-plastic constitutive model [Hibler, 1979] or an elastic-viscous-plastic model [Hunke and Dukowicz, 1997]. (However, in the latter, the elastic properties are chosen for numerical purposes.) This constitutive model is coupled to thermodynamic considerations through dependence of the ice strength on ice thickness. The ice thickness distribution varies in time due to mechanical motion and rearrangements of the ice, as well as growing and melting of ice.

Lindsay et al. [2003] compare RGPS data to model output, with and without data assimilated from buoy and SSMI-derived ice motion. The Pacific half of the Arctic Basin is analyzed for a 10 month period, November, 1997 to August, 1998. Both the RGPS data and the model output are manipulated to produce matched pairs of RGPS and model velocity and deformation values. These pairs are matched in location, time and in spatial scale. Mean and standard deviation of the velocity and deformation are computed and compared for the RGPS data and model output separately for the winter and summer months. The correlation between model estimates and RGPS data for velocity on a 320 m scale is good, especially with data assimilation. The correlation with deformation is worse. Several reasons are postulated for the relatively low deformation correlations. The large-scale velocity field might be represented well by the averaging procedures, but the smaller-scale spatial variations might not be so well represented. Errors may also occur in the location of model deformation events, and may arise from errors due to the data alignment process [Lindsay et al., 2003].

This paper attempts a simpler, more direct comparison between model output and RGPS data. The model predictions are based on the viscous-plastic constitutive model combined with a two-level ice thickness model. The next section reviews the mathematical model of sea ice. In order to evaluate the model, subregions of the Arctic have been identified for study. Actual displacements obtained from the RGPS are used to obtain boundary motion for the subregions. A boundary value problem is then solved to obtain the predicted ice motion in the interior of the region. The final sections of the paper describe the regions identified for study and the results of the numerical solution of the boundary value problem. The boundary value problem is solved over a short time, and the model output and RGPS data remain co-located in space and time. In this way, we hope to isolate the effects of the constitutive model, and gauge its efficacy in modeling deformation events and spatial variations in the velocity field.

THE SEA ICE MODEL

The mathematical model of sea ice is derived from considering the balance of linear momentum which is expressed by the following equation [Hibler, 1979]

$$m\frac{d\mathbf{v}}{dt} = \mathbf{F}^{\text{int}} + \mathbf{F}^{\text{ext}}. \tag{1}$$

In this equation, the time derivative is a material-time derivative, $d/dt = \partial/\partial t + \mathbf{v} \cdot \nabla$, where $\mathbf{v} = \mathbf{v}(\mathbf{x}, t)$ is the velocity field associated with the point $\mathbf{x}$ at time t. The quantity m is the ice mass per unit area, and $\mathbf{F}^{\text{int}}$ is the force due to variation in internal ice stress. External forces are described by the vector $\mathbf{F}^{\text{ext}}$ which includes Coriolis forces, air and water drag, and effects of sea surface tilt.

The internal force is given by the stress divergence, $\mathbf{F}^{\text{int}} = \nabla \cdot \boldsymbol{\sigma}$, where the stress is evaluated from a constitutive model. In this case the constitutive model is assumed to be a viscous-plastic model [Hibler, 1979]. Under this assumption, the stress $\boldsymbol{\sigma}$ is computed from the strain rate $\dot{\boldsymbol{\varepsilon}}$ according to the formula

$$\boldsymbol{\sigma} = 2\eta\dot{\boldsymbol{\varepsilon}} + [\zeta - \eta]\text{tr}(\dot{\boldsymbol{\varepsilon}})\boldsymbol{I} - \frac{1}{2}P\boldsymbol{I}. \tag{2}$$

The second order identity tensor is denoted by $\boldsymbol{I}$, and the trace of a tensor is indicated by the notation $\text{tr}(\cdot)$.

The viscosity coefficients η and ζ in this formulation are nonlinear functions of the strain rate and the ice strength P, $\eta = \eta(\dot{\boldsymbol{\varepsilon}}, P)$, and $\zeta = \zeta(\dot{\boldsymbol{\varepsilon}}, P)$. Specifically, $\zeta = P/2\Delta$, and $\eta = \zeta/e^2$ where e is the ratio of the principal axes of the elliptical yield surface [Hibler, 1977], and Δ depends on e and the strain rate

$$\Delta = [(\dot{\varepsilon}_{11}^2 + \dot{\varepsilon}_{11}^2)(1 + 1/e^2) + 4e^{-2}\dot{\varepsilon}_{12}^2 + 2\dot{\varepsilon}_{11}\dot{\varepsilon}_{22}(1 - 1/e^2)]^{1/2}. \tag{3}$$

As currently defined, the viscosity coefficients can become arbitrarily large for small strain rates. To avoid this difficulty, these coefficients are chosen to be the minimum of the values specified above and some large limiting values that depend on the ice strength. The limiting values are taken to be $\zeta_{\text{max}} = (2.5 \times 10^8 s)P$ and then $\eta_{\text{max}} = \zeta_{\text{max}}/e^2$.

The ice strength, P, is taken to be a function of the average ice thickness, h, and its compactness, A, according to the formula $P = P^* h \exp(-C(1 - A))$ which includes the fixed empirical constants $P^* = 5$ kPa and $C = 20$. As noted in the introduction, the ice thickness and compactness evolve due to thermodynamics and ice dynamics. Thermodynamics causes changes due to melting and freezing of ice. Dynamics cause changes through the creation of leads during divergent flow and closing of open water or ridging of ice during convergent flow. With these variables, one can keep track of two ice categories, thin and thick ice.

A simple model [Hibler, 1979] for the evolution of h and A consists of

$$\frac{dh}{dt} = -(\nabla \cdot \mathbf{v})h + S_h, \qquad \frac{dA}{dt} = -(\nabla \cdot \mathbf{v})A + S_A. \tag{4}$$

These equations are simple continuity equations for h and A with thermodynamic source terms S_h and S_A. The source terms are given by

$$S_h = f(h/A)A + (1 - A)f(0) \tag{5}$$

$$S_A = \begin{cases} (f(0)/h_0)(1 - A) & \text{if } f(0) > 0, \\ 0 & \text{if } f(0) < 0 \end{cases} + \begin{cases} 0 & \text{if } S_h > 0 \\ (A/2h)S_h & \text{if } S_h < 0. \end{cases} \tag{6}$$

The function $f(h)$ is the growth rate of ice of thickness h and $h_0 = 0.5$ m is a fixed thickness marking the cut-off between thin and thick ice.

ICE-MOTION TEST DATA

Three regions of the Arctic ice sheet have been identified for preliminary studies. Each region is 50 km $\times$ 50 km, and each region is briefly described in this section. The first region contains two leads. As the first region deforms, a small opening lead and a large shearing lead appear. The second region is quiet, and the third region contains the closing of the small lead in the first region, and the opening and shearing of the large lead in the first region. Thus, the first and third regions are the same Lagrangian points viewed at different times. Region one is day 135 of 2002, region three is on day 136. Region two is also day 136. A 5 km mesh is placed on each of these regions and the displacement of the mesh points is tracked. Figure 1 shows the undeformed and deformed meshes for each of the regions superimposed on the satellite images. The deformation in Figure 1(a) takes place over 20 hours, in Figure 1(b) it is over 1.7 hours and in Figure 1(c), the deformation takes place in 18.5 hours.

The next group of figures, Fig. 2, provides plots for divergence, shear and vorticity in each of the three regions. The divergence is $\partial u/\partial x + \partial v/\partial y$, shear is $((\partial u/\partial x - \partial v/\partial y)^2 + (\partial u/\partial y + \partial v/\partial x)^2)^{1/2}$, and the vorticity is $\partial v/\partial x - \partial u/\partial y$. In these formulae, the velocity is (u, v) and derivatives are approximated with finite differences. Each cell is colored by its value of divergence, vorticity or shear, using a fixed scale for all three regions. There is almost no activity in region 2 compared with the other two regions. Region 3 has a strong band of divergence, shear and vorticity running from southwest to northeast, corresponding to the opening and shearing of the large lead. The closing of the small lead is not visible in these fields. The deformation pattern for region 1 is the most complex of the three regions. The caption to Fig. 2 also contains statistics about the deformation.

SOLUTION OF THE BOUNDARY VALUE PROBLEM

The displacement of each grid point in Fig. 1 is known from the satellite imagery. In particular, the displacement of the boundary nodes of the initially square regions shown in the figure are known. Thus, a well-defined mathematical problem can be posed using these known boundary displacements in conjunction with the momentum balance equation (1). Since we propose to examine the ice motion for small regions only over approximately one day, and since the boundary motion includes effects from the external forcing, we drop the term $\mathbf{F}^{\text{ext}}$ from equation (1) and just consider the internal forces. The internal forces come from the stress divergence and the stress is determined from the viscous-plastic constitutive model. The mass m per unit area is given by the density of the ice (per unit volume) times the average thickness of the ice h/A.

The regions under consideration are observed on days 135-6. In mid-May, the rate of ice growth $f(h)$ is nearly constant at about 0.165 cm/day for all thick ice. Ice forms

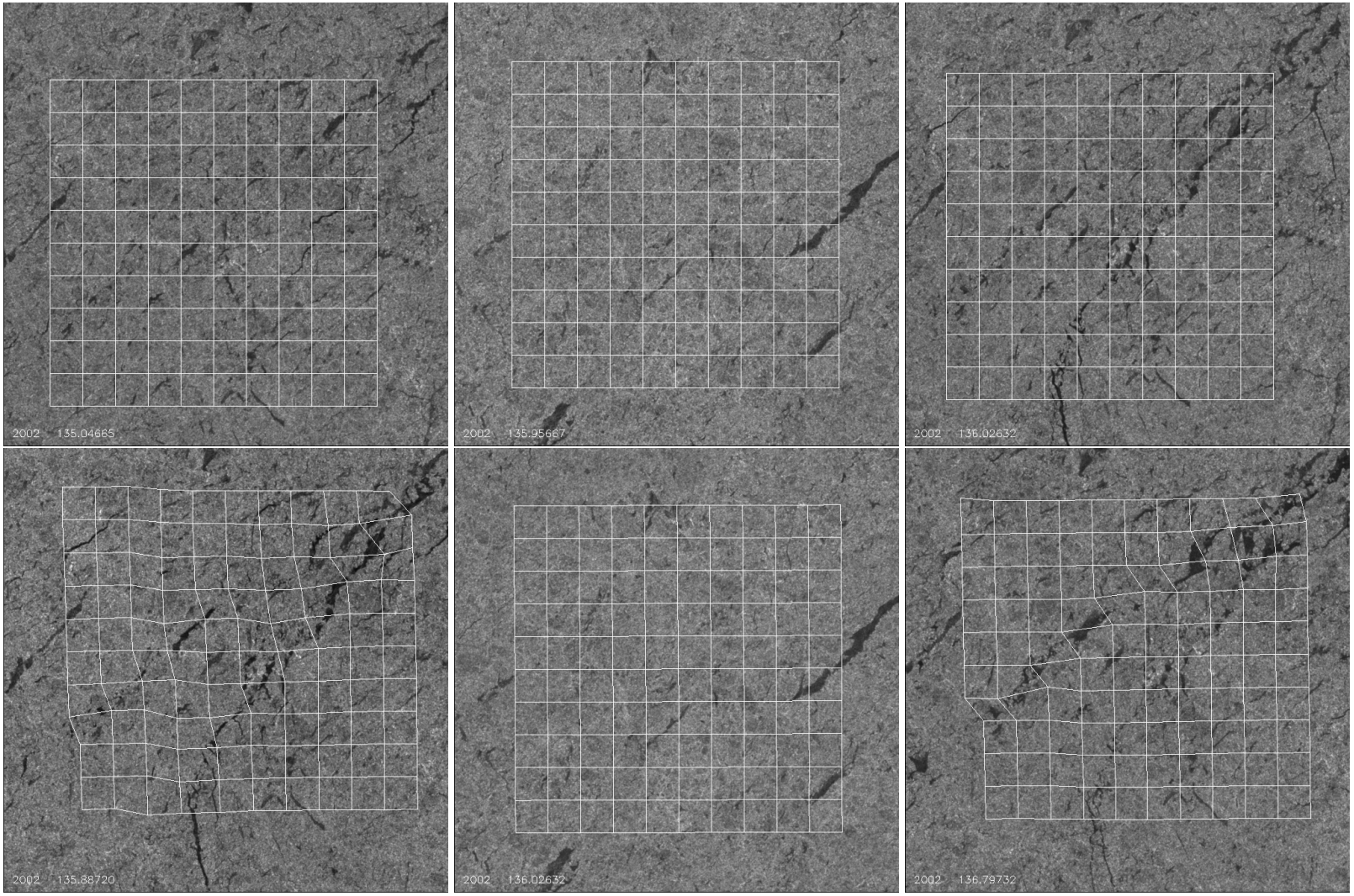

(a) (b) (c)

Figure 1: Undeformed (top) and deformed (bottom) meshes for the three regions. The deformation occurs over (a) 20 hours, (b) 1.7 hours, and (c) 18.5 hours.

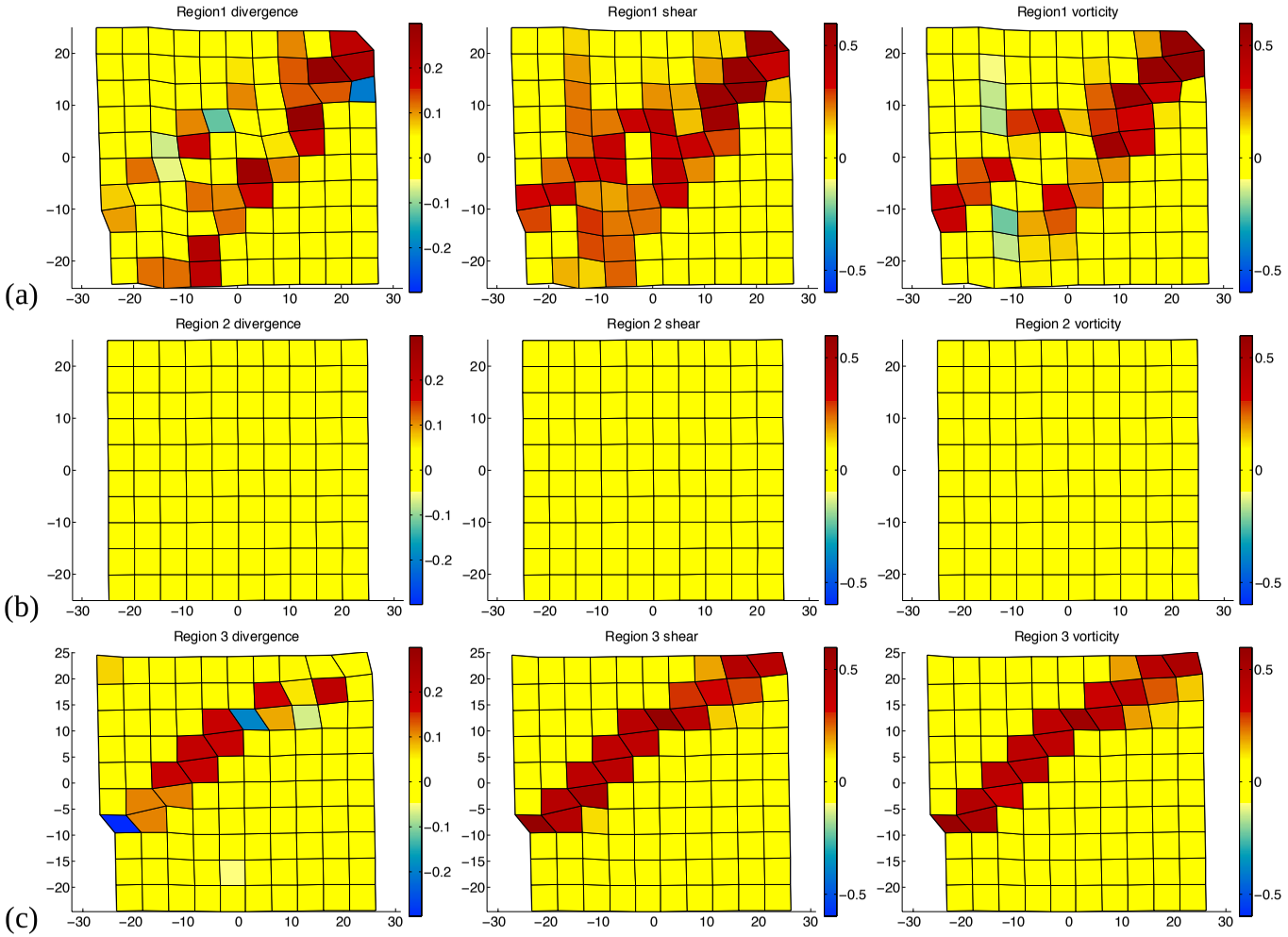

Figure 2: Plots of divergence, shear and vorticity in (a) region one (b) region two and (c) region three. The left column is divergence, the center column is shear and the right column is vorticity. The mean and standard deviation for the divergence is (a) 0.043, 0.08 (b) -0.013, 0.096 (c) 0.013, 0.086; the mean and standard deviation for the shear is (a) 0.15, 0.16 (b) 0.14, 0.13 (c) 0.12, 0.20; and the mean and standard deviation for the vorticity is (a) 0.11, 0.17 (b) 0.14, 0.16 (c) 0.12, 0.20; in units of day^{-1}.

at a rate $f(0) = 0.65$ cm/day by freezing open water [Thorndike et al., 1975]. These values are used in the thickness model (6). Since $f(0) > 0$ and $S_h > 0$ for these growth rates, the source term for A reduces to $S_A = (f(0)/h_0)(1 - A)$, indicating the rate at which open water is converted to ice. Now, given the value of $\nabla \cdot \mathbf{v}$ for a time step, the value of h and A can be obtained by exactly integrating equations (4) over the step.

The boundary value problem is solved using the material-point method (MPM) [Sulsky et al., 1994, 1995; Sulsky and Schreyer, 1996]. In this implementation, the computational grid is Lagrangian with the initial size of the elements the same as the RGPS grid and with one material point per element. This form makes the method essentially the same as a Lagrangian finite element method with one-point integration. The time step, Δt, is chosen for numerical stability of an explicit update so that, for all elements, $\Delta t < m\Omega/(2\eta)$, where Ω is the area of the computational element.

Results of the simulations are shown in Fig. 3 where the observed and computed velocity of the nodes are compared. An error measure is obtained by computing, for each grid point i, the quantity ε_i which is the magnitude of the vector difference of the observed and computed velocity. A single, dimensionless measure is obtained by the RMS error, $\sqrt{\sum_i \varepsilon_i^2}$, scaled by the RMS magnitude of the observed speed. The result is an error of 0.35, 0.51 and 0.30, for regions one, two and three; respectively. A correlation coefficient is also computed for the velocity field (with the velocity vector treated as a complex number) and reported in the figure caption.

Further comparison can be made by examining the computed divergence, shear and vorticity for regions one and three. (Region two is omitted since there is no discernible divergence, vorticity or shear in the observations or simulations.) Fig. 4 shows plots of these quantities for the numerical simulations that can be compared to the observed values displayed in Fig. 2. For region three, the computed solution picks up a reasonable representation of the shear and vorticity, but underestimates the divergence. Specifically, much less opening is predicted. The deformation pattern in region one is much harder to capture, aspects of the shear and vorticity in the upper right corner of the region appear in the simulations but not those in the lower right corner. Again, less opening is predicted. A dimensionless measure of the differences is computed by taking the RMS difference in the computed and predicted values divided by the RMS magnitude of the observed data. For region one, the divergence error is 0.85, the shear error is 0.58 and the vorticity error is 0.65. For region three, the divergence error is 0.86, the shear error is 0.46 and the vorticity error is 0.43.

The strength of the ice was reduced by an order of magnitude and the model results recomputed. The statistics changed insignificantly. The methods described can be used to test the model predictions, but apparently the boundary value problem constrains the motion too much to test the rheology.

CONCLUSIONS

High correlation between ice speeds determined from RGPS observations and model output is observed. However, the RMS error is more sensitive to outlying data, and for

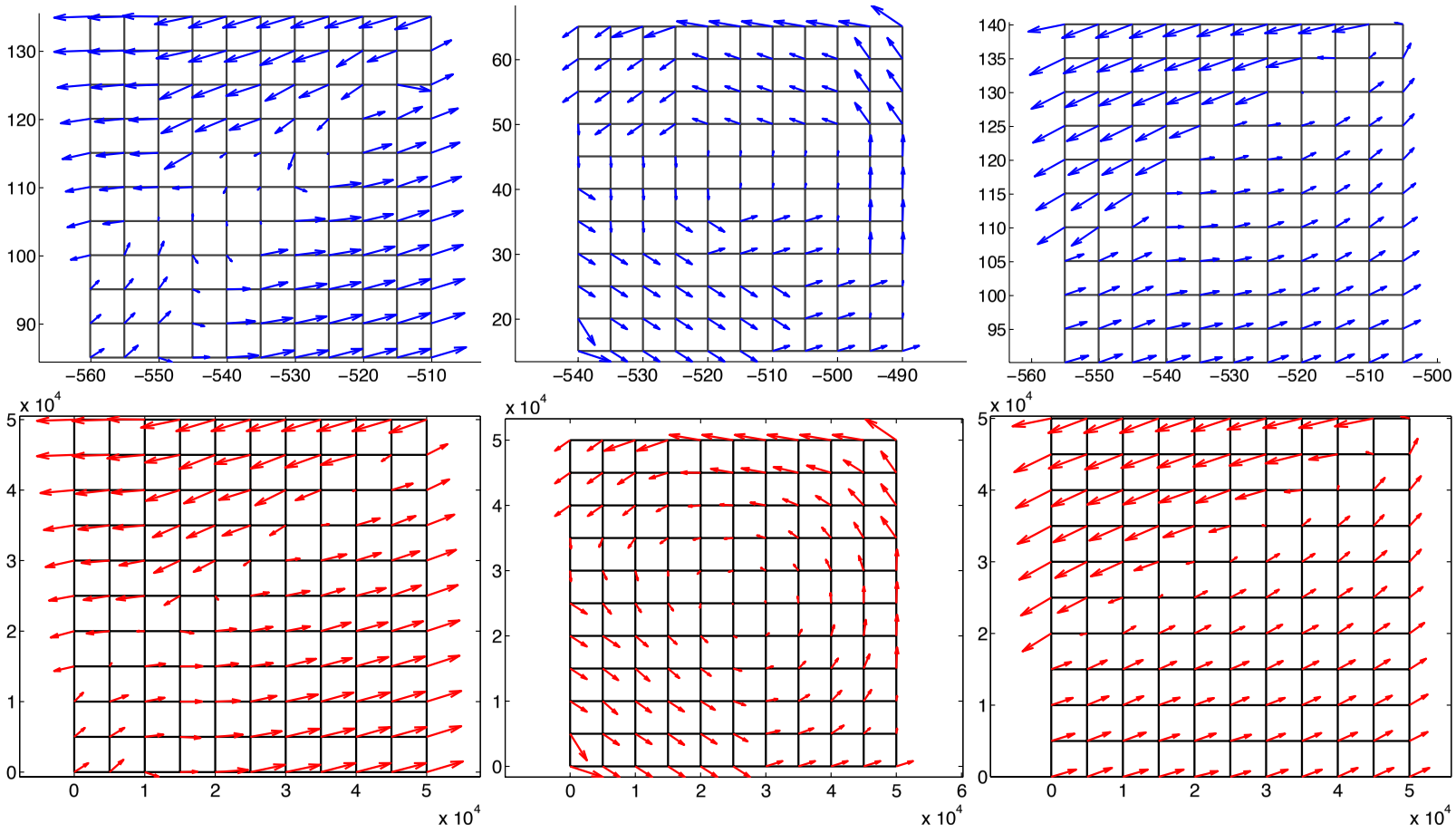

(a) (b) (c)

Figure 3: Observed (top) and computed (bottom) velocity of the grid nodes for (a) region one, (b) region two, and (c) region three. For the observed, RGPS data, the mean speed and its standard deviation are (a) 1.96, 0.73 (b) 1.62, 0.63 (c) 1.94, 0.76. For the computed, model data, the mean speed and standard deviation are (a) 1.97, 0.62 (b) 1.49, 0.68 (c) 1.89, 0.78. The units are km/day. The average translational motion has been removed from both the observations and model data. The correlation coefficients are (a) 0.81, (b) 0.82, and (c) 0.91.

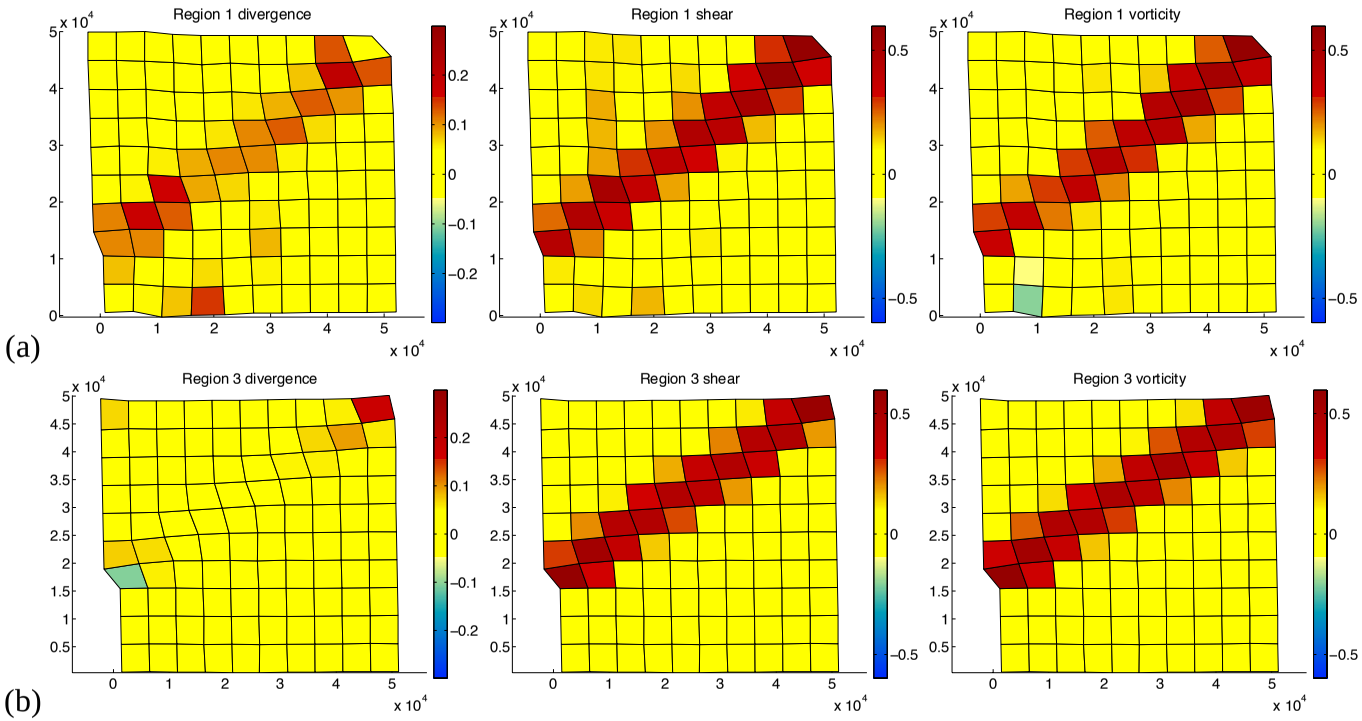

Figure 4: Plots of simulated divergence, shear and vorticity in (a) region one and (b) region three. The left column is divergence, the center column is shear and the right column is vorticity. The mean and standard deviation for the divergence is (a) 0.043, 0.046 (b) 0.013, 0.030; the mean and standard deviation for the shear is (a) 0.13, 0.15 (b) 0.11, 0.16; and the mean and standard deviation for the vorticity is (a) 0.11, 0.16 (b) 0.12, 0.16. The units are day^{-1}. The correlation coefficients for the divergence are (a) 0.35 (b) 0.52, for the shear are (a) 0.68 (b) 0.85, and for the vorticity are (a) 0.69 (b) 0.86.

the speed, the relative RMS error is found to be 30-50%. As in [Lindsay et al., 2003], high correlation of the speed does not imply accuracy of the derived deformation. The correlation between observed and computed shear and vorticity are lower than that for the speed, but still reasonable. The correlation for the divergence is relatively lower. The discrepancy in the divergence is highlighted by the large RMS error of 84-86%. It is evident from contour plots that the amount of opening is under predicted in the numerical simulations. If systematic, under-estimation of opening would lead to under estimation of the amount of ice production in climatological studies.

ACKNOWLEDGMENT

This material is based upon work supported by the National Science Foundation under Grant No. DMS-0222253.

REFERENCES

Hibler, W. D. (1977). Viscous sea ice law as a stochastic average of plasticity. *Journal Of Geophysical Research-Oceans And Atmospheres*, 82(27):3932 – 3938.

Hibler, W. D. (1979). Dynamic thermodynamic sea ice model. *Journal Of Physical Oceanography*, 9(4):815 – 846.

Hunke, E. C. and Dukowicz, J. K. (1997). An elastic-viscous-plastic model for sea ice dynamics. *Journal Of Physical Oceanography*, 27(9):1849 – 1867.

Kwok, R. (1998). The radarsat geophysical processor system. In *Analysis Of SAR Data Of The Polar Oceans: Recent Advances*, pages 235–257. Springer-Verlag.

Kwok, R., Rothrock, D. A., Stern, H. L., and Cunningham, G. F. (1995). Determination of ice age using lagrangian observations of ice motion. *IEEE Trans. Geosci. Remote Sens.*, 33(2):392–400.

Lindsay, R. W., Zhang, J., and Rothrock, D. A. (2003). Sea-ice deformation rates from satellite measurements and in a model. *Atmosphere-Ocean*, 41(1):35 – 47.

Sulsky, D., Chen, Z., and Schreyer, H. L. (1994). A particle method for history-dependent materials. *Comput. Methods Appl. Mech. Engrg.*, 118:179–196.

Sulsky, D. and Schreyer, H. L. (1996). Axisymmetric form of the material point method with applications to upsetting and Taylor impact problems. *Comput. Meths. Appl. Mech. Engrg.*, 139:409–429.

Sulsky, D., Zhou, S.-J., and Schreyer, H. L. (1995). Application of a particle-in-cell method to solid mechanics. *Comput. Phys. Commun.*, 87:236–252.

Thorndike, A., Rothrock, D., Maykut, G., and Colony, R. (1975). The thickness distribution of seaice. *Journal Of Geophysical Research*, 80(33):4501–4513.